DRAFT VERSION NOVEMBER 2, 2015
Preprint typeset using LaTeX style emulateapj v. 26/01/00

EXTREMES OF THE JET–ACCRETION POWER RELATION OF BLAZARS, AS EXPLORED BY *NUSTAR*

T. SBARRATO[1], G. GHISELLINI[2], G. TAGLIAFERRI[2], M. PERRI[3,4], G. M. MADEJSKI[5], D. STERN[6], S. E. BOGGS[7], F. E. CHRISTENSEN[8], W. W. CRAIG[8,9], C. J. HAILEY[10], F. A. HARRISON[11], W. W. ZHANG[12]

Draft version November 2, 2015

ABSTRACT

Hard X–ray observations are crucial to study the non–thermal jet emission from high–redshift, powerful blazars. We observed two bright $z > 2$ flat spectrum radio quasars (FSRQs) in hard X–rays to explore the details of their relativistic jets and their possible variability. S5 0014+81 (at $z = 3.366$) and B0222+185 (at $z = 2.690$) have been observed twice by the *Nuclear Spectroscopic Telescope Array* (*NuSTAR*) simultaneously with *Swift*/XRT, showing different variability behaviours. We found that *NuSTAR* is instrumental to explore the variability of powerful high–redshift blazars, even when no γ–ray emission is detected. The two sources have proven to have respectively the most luminous accretion disk and the most powerful jet among known blazars. They are located at the extreme end of the jet–accretion disk relation previously found for γ–ray detected blazars.

Subject headings: galaxies: active – quasars: general – X–rays: general – quasars: individual (B0222+185, S5 0014+813)

1. INTRODUCTION

Blazars are active galactic nuclei (AGN) with their broad–band emission dominated by the relativistic jet, oriented close to our line of sight. The two humps that characterise their spectral energy distribution (SED) are the signature of this relativistically beamed emission. They are attributed to synchrotron (at lower frequencies) and inverse Compton (at high frequencies) processes, and peak in the sub–millimeter and X– to γ–ray, respectively. The electron population involved in the inverse Compton emission is thought to interact either with the synchrotron photons involved in the lower–frequency emission, or with photons coming from structures external to the relativistic jet (synchrotron self–Compton, SSC, or external Compton, EC, emissions, respectively). The latter is likely the primary process in sources that present a pronounced dominance of the higher frequencies hump over the synchrotron one. This usually happens in the most powerful blazars, i.e. the flat–spectrum radio quasars (FSRQs). These sources are thought to have more sources of seed photons for an EC process (i.e. accretion disk, broad line region, torus), compared to the BL Lacertae objects (BL Lacs) that have weak or absent broad lines and no accretion or torus emission (see e.g. Chiaberge, Capetti & Celotti 1999; Ghisellini et al. 2011, Sbarrato et al. 2012).

The most immediate signature of the blazar nature of an AGN is its emission in the γ–rays. The high–energy hump in the blazar SED, in fact, usually peaks at tens or hundreds of MeV, and therefore it can be easily observed with γ–ray telescopes, such as the Large Area Telescope (LAT) onboard the *Fermi Gamma–Ray Space Telescope* (Atwood et al. 2009). *Fermi*/LAT provides an all–sky survey in the γ–rays, that ensures a clear classification of the blazar candidates. Nevertheless, at higher redshifts, *Fermi*/LAT is less efficient in detecting blazars, even those with a very large bolometric luminosity. This is because the most powerful blazars have their high energy peak at $\sim$MeV energies or below, and this peak is seen redshifted. This is the reason why the fraction of high redshift blazars (i.e. at $z > 2$) detected in the hard X–rays by the Burst Alert Telescope (BAT) onboard the *Swift* satellite is much larger than for *Fermi*/LAT (see Ajello et al. 2009, Ghisellini et al 2010a).

Indeed, blazars observed so far show a trend: the humps in the SEDs of the more powerful ones peak at lower frequencies as compared to less powerful blazars. This trend is known as the "blazar sequence" (Fossati et al. 1998, but see also Giommi et al. 2012). As a result, it is likely that the most powerful and distant blazars cannot be detected by *Fermi*/LAT. Hard X–ray instruments, instead, like *Swift*/BAT and now the *Nuclear Spectroscopic Telescope Array* (*NuSTAR*; Harrison et al. 2013), are the most suitable instruments now available to investigate jet emission in the most powerful blazars at $z \sim 2 - 3$.

In this paper we report on observations of S5 0014+81 (at $z = 3.366$) and B0222+185 ($z = 2.690$) by *NuSTAR*. These two blazars have been previously detected in the 3–year all–sky survey of *Swift*/BAT (Ajello et al. 2009, see also Ajello et al. 2012 and Baumgartner et al. 2013), and are amongst the most powerful blazars ever observed. As with other pow-

[1]Dipartimento di Fisica "G. Occhialini", Università di Milano – Bicocca, piazza della Scienza 3, I–20126 Milano, Italy; tullia.sbarrato@unimib.it
[2]INAF – Osservatorio Astronomico di Brera, via E. Bianchi 46, I–23807 Merate, Italy.
[3]ASI Science Data Center, via del Politecnico, I–00133 Roma, Italy
[4]INAF – Osservatorio Astronomico di Roma, via Frascati 33, I–00040 Monteporzio Catone, Italy
[5]Kavli Institute for Particle Astrophysics and Cosmology, SLAC National Accelerator Laboratory, Menlo Park, CA 94025, USA
[6]Jet Propulsion Laboratory, California Institute of Technology, Pasadena, CA 91109, USA
[7]Space Sciences Laboratory, University of California, Berkeley, CA 94720, USA
[8]DTU Space - National Space Institute, Technical University of Denmark, Elektrovej 327, 2800 Lyngby, Denmark
[9]Lawrence Livermore National Laboratory, Livermore, CA 94550, USA
[10]Columbia Astrophysics Laboratory, Columbia University, New York, NY 10027, USA
[11]Cahill Center for Astronomy and Astrophysics, California Institute of Technology, Pasadena, CA 91125, USA
[12]NASA Goddard Space Flight Center, Greenbelt, MD 20771, USA

erful and high–redshift FSRQs, their optical flux shows contributions due to thermal emission from the accretion disk, particularly prominent in S5 0014+813, whose luminosity reaches $\sim 10^{48}$ erg s^{-1} (Ghisellini et al. 2010a). For both sources, the *Swift*/BAT spectrum together with the *Fermi*/LAT upper limit already constrained the location of the high energy peak, but with a relatively large uncertainty given the poor spectral slope determination of *Swift*/BAT. This motivated the *NuSTAR* observations.

In this work, we adopt a flat cosmology with $H_0 = 70$ km s^{-1} Mpc^{-1} and $\Omega_{\rm M} = 0.3$.

2. OBSERVATIONS AND DATA ANALYSIS

2.1. *NuSTAR observations*

The *NuSTAR* satellite observed S5 0014+81 on 2014 December 21 (obsID 60001098002) and on 2015 January 23 (obsID 60001098004) for total net exposure times of 31.0 ks and 36.4 ks, respectively. B0222+185 was observed by *NuSTAR* on 2014 December 24 (obsID 60001101002) and on 2015 January 18 (obsID 60001101004). The total net exposure times were 32.0 ks and 37.4 ks, respectively.

The Focal Plane Module A (FPMA) and Focal Plane Module B (FPMB) data sets were first processed with the *NuSTARDAS* software package (v.1.4.1) jointly developed by the ASI Science Data Center (ASDC, Italy) and the California Institute of Technology (Caltech, USA). Event files were calibrated and cleaned with standard filtering criteria using the *nupipeline* task (version 20150316) of the *NuSTAR* CALDB.

The two sources were well detected in the *NuSTAR* 3–79 keV energy band. In both cases the FPMA and FPMB spectra of the target were extracted from the cleaned event files using a circle of 20 pixel (~ 49 arcsec) radius, while the background was extracted from nearby circular regions of 40 pixel radius. The ancillary response files were generated with the *numkarf* task, applying corrections for the PSF losses, exposure maps and vignetting. All spectra were binned to ensure a minimum of 30 counts per bin.

2.2. *Swift observations*

The *Swift* satellite observed S5 0014+81 on 2014 December 21 (obsIDs 00080003001) and on 2015 January 23 (obsID 00080003002) while B0222+185 was observed on 2014 December 24 (obsID 00080243001) and on 2015 January 18 (00080243002). The total net exposure times were 6.5 ks (December 2014) and 6.6 ks (January 2015) for S5 0014+81 and 4.9 ks (December 2014) and 5.1 ks (January 2015) for B0222+185.

2.2.1. *XRT observations*

Swift/XRT (Burrows et al. 2005) observations were carried out using the Photon Counting (PC) CCD readout mode and in the four observations the sources were well detected in the 0.3-10 keV XRT energy band. The XRT data sets were first processed with the XRTDAS software package (v.3.0.0) developed at the ASI Science Data Center (ASDC) and distributed by HEASARC within the HEASoft package (v. 6.16). In particular, event files were calibrated and cleaned with standard filtering criteria with the *xrtpipeline* task using the calibration files available in the version 20140709 of the *Swift*/XRT CALDB.

The energy spectra were then extracted from the calibrated and cleaned event files. Events for the source spectral analysis were selected within a circle of 20 pixel (~ 47 arcsec) radius, enclosing about 90% of the PSF, while the background was extracted from a nearby circular region of 80 pixel radius. The ancillary response files were generated with the *xrtmkarf* task, applying corrections for the PSF losses and CCD defects using the cumulative exposure map. The source spectra were binned to ensure a minimum of 30 counts per bin.

2.2.2. *UVOT observations*

Swift/UVOT (Roming et al. 2005) observations were performed with all six optical and UV lenticular filters (namely $V, U, B, W1, M2, W2$). We performed aperture photometry for all filters in all the observations using the standard UVOT software distributed within the HEAsoft package (version 6.16) and the calibration included in the latest release of the CALDB. Counts were extracted from apertures of 5 arcsec radius for all filters and converted to fluxes using the standard zero points (Poole et al. 2008). The fluxes were then de–reddened using the appropriate values of $E(B-V)$ taken from Schlegel et al. (1998) and Schlafly et al. (2011) with $A_\lambda/E(B-V)$ ratios calculated for UVOT filters using the mean Galactic interstellar extinction curve from Fitzpatrick (1999). No variability was detected within single exposures in any filter. The processing results were carefully verified, checking for possible contaminations from nearby objects within the source apertures and from objects falling within the background apertures.

2.3. *X–ray spectral analysis*

The spectral analysis of the December 2014 and January 2015 *NuSTAR* and *Swift*/XRT simultaneous observations of S5 0014+81 and B0222+185 were performed using the XSPEC package. In all four observations a broken power–law model with an absorption hydrogen–equivalent column density fixed to the Galactic value of 1.35×10^{21} cm^{-2} (S5 0014+81) and 9.4×10^{20} cm^{-2} (B0222+185) (Kalberla et al. 2005) was found to provide a good description of the observed spectra in the 0.3–79 keV energy band. The inter–calibration factors between the three instruments (*NuSTAR*/FPMA, *NuSTAR*/FPMB and *Swift*/XRT) were taken into account adding a multiplicative constant (kept to 1 for *NuSTAR*/FPMA) to the spectral model. We found values in the 2% range for *NuSTAR*/FPMB and in the 10% range for *Swift*/XRT which are consistent with the cross–calibration uncertainties for the instruments (Madsen et al. 2015). The results of the spectral fits are shown in Table 1, and Figure 1 shows the X–ray spectra of the two sources.

We also tried a simpler spectral model, namely a single power–law with an absorption hydrogen–equivalent column density fixed to the Galactic value. However, for all four observations we found significantly higher χ^2 values, thus confirming the existence of an intrinsic spectral curvature within the observed 0.3–79 keV energy band.

3. BLACK HOLE MASS ESTIMATE

The black hole mass of a blazar is an important feature to characterise it. When optical or infrared spectra are not available, the virial mass estimate method cannot be applied. At high redshift, the available lines to apply such a method are also less reliable. With a good photometric coverage of the UV–optical–IR band, instead, the accretion disk emission can be fitted, and the black hole mass can be estimated from this fitting process (Calderone et al. 2013).

[13] www.asdc.asi.it

S5 0014+81

Date	Γ_1	Γ_2	$E_{\rm break}$ keV	$F_{0.5-2\rm kev}$ erg cm^{-2} s^{-1}	$F_{2-10\rm kev}$ erg cm^{-2} s^{-1}	$F_{10-50\rm kev}$ erg cm^{-2} s^{-1}	χ^2 / dof
2014 Dec 1	$1.18^{+0.22}_{-0.27}$	1.72 ± 0.05	$2.22^{+0.83}_{-0.58}$	1.4×10^{-12}	3.8×10^{-12}	6.0×10^{-12}	151.8 / 136
2015 Jan 23	$0.64^{+0.44}_{-0.61}$	1.65 ± 0.05	$1.61^{+0.61}_{-0.34}$	1.3×10^{-12}	3.62×10^{-12}	6.36×10^{-12}	133.2 / 147

B0222+185

Date	Γ_1	Γ_2	$E_{\rm break}$ keV	$F_{0.5-2\rm kev}$ erg cm^{-2} s^{-1}	$F_{2-10\rm kev}$ erg cm^{-2} s^{-1}	$F_{10-50\rm kev}$ erg cm^{-2} s^{-1}	χ^2 / dof
2014 Dec 24	$1.10^{+0.19}_{-0.10}$	$1.56^{+0.09}_{-0.03}$	$4.77^{+2.61}_{-0.55}$	2.6×10^{-12}	1.2×10^{-11}	2.7×10^{-11}	483.6 / 504
2015 Jan 18	1.06 ± 0.12	$1.69^{+0.05}_{-0.04}$	$4.69^{+0.83}_{-0.56}$	1.9×10^{-12}	8.3×10^{-12}	1.5×10^{-11}	406.8 / 400

TABLE 1

PARAMETERS OF THE X–RAY SPECTRAL ANALYSIS, FROM THE SIMULTANEOUS FIT OF *NuSTAR* AND *Swift*/XRT. THE ERRORS ARE AT 90% LEVEL OF CONFIDENCE FOR ONE PARAMETER OF INTEREST. FLUXES ARE CORRECTED FOR GALACTIC ABSORPTION.

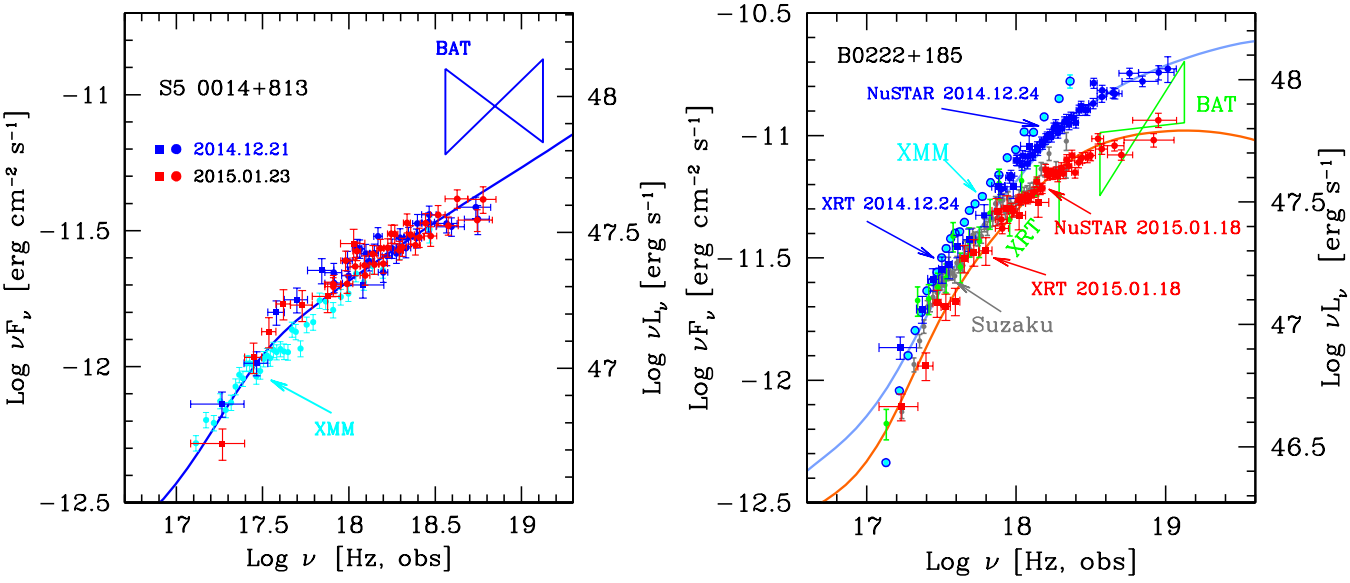

FIG. 1.— X–ray spectra of S5 0014+813 and B0222+185, along with the SED models described in the text with parameters as in Tables 2 and 3 (shown in solid blue and red lines). In both panels, new *Swift*/XRT and *NuSTAR* data are respectively filled squares and circles. The December 2014 observations are in blue, the January 2015 ones are in red. *Left panel*: X–ray spectrum of S5 0014+813. Archival *Swift*/BAT data are shown in blue, while the cyan circles are archival XMM data, as labelled. These data were used and commented in detail in Ghisellini et al. (2009; 2010a). *Right panel*: X–ray spectrum of B0222+185. Archival data are shown in green (*Swift*/XRT and BAT), grey (*Suzaku*) and cyan (*XMM–Newton*). They were shown and described in detail in Ghisellini et al. (2009).

The *Swift*/UVOT photometric data, along with archival data from the ASI Science Data Center (ASDC[13]) allow us to cover the optical–UV band of the SEDs. The first feature to notice in the IR–optical–UV SEDs of the two blazars is the absorption at frequencies higher than $\log(\nu/\mathrm{Hz}) = 15.4$ rest frame. This is the Lyα forest, due to intervening clouds absorbing hydrogen Lyα photons, and affects wavelengths shortward of 1216 Å. The bluer UVOT bands fall in this frequency range in the case of S5 0014+318 and B0222+185, and in fact only upper limits could be derived for those photometric bands. At frequencies lower than this prominent absorption feature, though, a peak in the SEDs is clearly visible. Below this peak, the optical flux decreases with frequency, suggesting a power–law trend, especially in S5 0014+813. This is the clear signature of an accretion disk, which can be fitted with a simple Shakura–Sunyaev model (Shakura & Sunyaev 1973; Calderone et al. 2013; Sbarrato et al. 2013). At lower frequencies, another feature is evident from the IR–optical–UV SEDs of these two sources: the *WISE* (Wright et al. 2010) IR bands show an increase of the flux, that breaks the power–law–like trend in the optical. This is likely the signature of the IR emission from a dusty torus around the nucleus.

With these premises, a reliable way to estimate the black hole mass of S5 0014+318 and B0222+185 is to fit their IR–optical–UV SEDs with a simple model of accretion disk emission. We applied the radiatively efficient, geometrically thin, optically thick Shakura & Sunyaev (1973) model. Assuming a standard radiative efficiency $\eta = 0.08$, only two free parameters are left to be fitted: the accretion rate $\dot{M}$, that can be traced by the intrinsic disk luminosity $L_\mathrm{d} = \eta \dot{M} c^2$, and the black hole mass M_BH itself. We can constrain the overall disk luminosity thanks to the visibility of the peak of the disk emission, with some consideration regarding its anisotropic properties (as throughly explained by Calderone et al. 2013):

1. according to the Shakura–Sunyaev model, the peak luminosity $\nu_p L_{\nu_p}$ corresponds to half the total observed luminosity $L_\mathrm{obs} = 2\nu_p L_{\nu_p}$.

2. the observed luminosity depends on the viewing angle of the accretion disk:
$$L_\mathrm{obs} = 2\cos\theta_\mathrm{v} L_\mathrm{d} \quad (1)$$
where L_d is the intrinsic total luminosity emitted by the accretion disk. In the case of a blazar $L_\mathrm{obs} \simeq 2L_\mathrm{d}$ since we see the accretion disk face–on.

We can therefore derive the intrinsic total luminosity from the peak luminosity of our sources:
$$L_\mathrm{d} = \frac{\nu_p L_{\nu_p}}{\cos\theta_\mathrm{v}} \simeq \nu_p L_{\nu_p}. \quad (2)$$
This means that in the case of these two sources, L_d is constrained by observations, and only M_BH is left as a free parameter to be derived with the IR–optical–UV SED fitting.

We find that both sources have large black hole masses and are fast accreting, even if not super–Eddington. We derive $M_\mathrm{BH} = 1.5 \times 10^9 M_\odot$ and $L_\mathrm{d} = 5.3 \times 10^{46}$ erg s^{-1} for B0222+185 and $M_\mathrm{BH} = 7.5 \times 10^9 M_\odot$ and $L_\mathrm{d} = 8.3 \times 10^{47}$erg s^{-1} for S5 0014+813. These values are significantly smaller than what was derived in Ghisellini et al. (2009 and 2010a). For S5 0014+813 the reason is due to i) the better coverage of the IR band achieved with *WISE* data and ii) neglecting the optical data taken from Bechtold et al. (1994). We now prefer to discard those data because the derivation of flux and luminosities are not sufficiently clear in that paper.

For B0222+185, the smaller values of M_BH and L_d are due to the new infrared data (not available in the previous work), that now help more accurately constrain the peak frequency of the disk emission.

4. MODELLING THE BROAD–BAND SED

Figure 2 shows that both S5 0014+318 and B0222+185 have overall SEDs characterised by a prominent high–energy component, that along with the characteristic flat and intense radio luminosity is attributed to non–thermal emission from a relativistic jet. In the IR–optical–UV range of both sources, the SEDs are dominated by thermal emission attributed to the accretion disk, as discussed in Section 3.

Not being detected in the γ–rays by *Fermi*/LAT, X–ray data are necessary to study the non–thermal high–energy emission of S5 0014+318 and B0222+185. Specifically, *NuSTAR* data are crucial for understanding the X–ray spectral profile and possible variability in this kind of high–redshift source, as can be seen in Figure 1. X–ray data contribute significantly to the modelling of the broad–band SEDs of the two sources (Figure 2).

To interpret the SEDs of the two sources, we used a leptonic one–zone emitting model, fully described in Ghisellini & Tavecchio (2009). We refer to the original paper for details, providing here only a very brief description of the most important features of the models. The emitting source is assumed to be a spherical region in which relativistic electrons emit by synchrotron and inverse Compton processes. This homogeneous spherical blob is assumed to be located at a distance R_diss from the central black hole, moving with a bulk Lorentz factor Γ at an angle θ_v from our line–of–sight. Relativistic electrons are injected throughout the source, with a power P'_i as measured in the comoving frame. The energy distribution $Q(\gamma)$ of the injected electrons is a smoothly broken power law with slopes s_1 and s_2 (defined as $Q(\gamma) \propto \gamma^{-s}$) below and above the random Lorentz factor γ_b. Note that, even if $Q(\gamma)$ is a broken power law, N_γ derived through the continuity equation maintains a break, albeit smoother than the injected broken power law. This produces a gently curved spectrum, as shown in Figure 1. The broad line region is located at a distance $R_\mathrm{BLR} = 10^{17} L_{\mathrm{d},45}^{1/2} \mathrm{cm}$ from the black hole, while the infrared emitting torus is at $R_\mathrm{torus} = 10^{18} L_{\mathrm{d},45}^{1/2} \mathrm{cm}$. $L_{\mathrm{d},45}$ is the accretion disk luminosity in units of $10^{45}\,\mathrm{erg\,s^{-1}}$, and it is derived as in Section 3, together with the central black hole mass. The values of the parameters adopted for the models are reported in Table 2.

Table 3 reports the different forms of the power carried by the jet: the power P_r spent in producing the radiation we observe, the Poynting flux P_B, the power associated to the bulk motion of relativistic electrons (P_e) and cold protons (P_p), assuming one proton per relativistic electron. This assumption is consistent with independent results on blazar and GRB jets by Nemmen et al. (2012). They found that the total jet power for both classes is ten times the radiative power P_rad, i.e. similar to what we find in this work (see Table 3). Different proton–to–relativistic electron ratios were explored by Sikora & Madejski (2000), who found that the relativistic pairs must be less than 10-20 per proton. With this combination, the total jet power can result equal to or even less than the radiative power, that instead is only a part of the total power carried by the jet, and hence should be a lower limit to the total P_j (Ghisellini 2012;

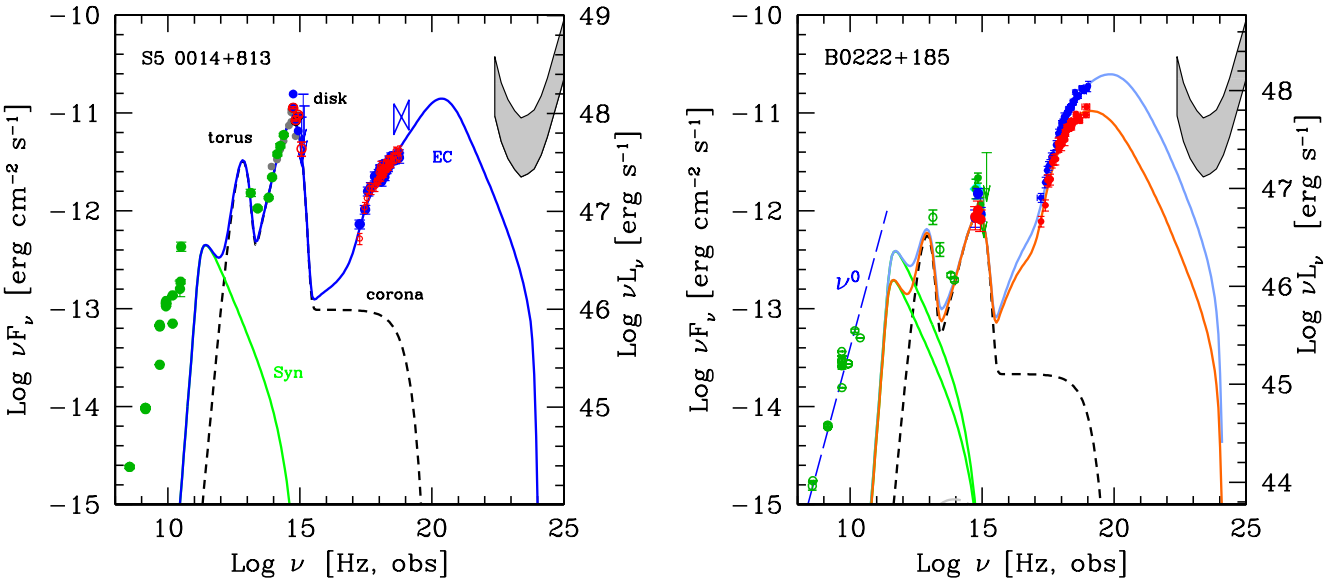

FIG. 2.— Broad–band SEDs of S5 0014+813 and B0222+185 along with the models discussed in the text and parametrised as in Tables 2 and 3. In both panels, the grey stripe is the 5σ *Fermi*/LAT sensitivity limit, calculated for 5 years (lower edge) and 1 year of operations (upper edge). New *Swift*/UVOT, *Swift*/XRT and *NuSTAR* data for the two observation periods are red (January 2015) and blue (December 2014) circles. *Left panel*: S5 0014+813 SED with its broad–band model (blue solid line). The green solid line is the self–absorbed synchrotron emission, while the thermal emission from accretion disk, torus and X–ray corona is shown with the dashed black line. Green data points in radio and IR are from the literature (for details see Ghisellini et al. 2009). Archival *Swift*/BAT data are shown in blue. *Right panel*: SED of B0222+185 with the two models corresponding to the low state (orange solid line) and the high state (blue solid line). Synchrotron emission in the two states are both shown with green solid lines. The thermal emission from the nuclear region (black dashed line) does not vary between the two states. Green empty circles are archival data (from ASDC).

Source	z	$M_{\rm BH}$	$R_{\rm diss}$	$R_{\rm BLR}$	$R_{\rm T}$	$L_{\rm d}$	$L_{\rm d}/L_{\rm Edd}$	Γ	$\theta_{\rm v}$	$P'_{\rm i}$	B	$\gamma_{\rm b}$	$\gamma_{\rm max}$	$\gamma_{\rm cool}$	s_1	s_2
[1]	[2]	[3]	[4]	[5]	[6]	[7]	[8]	[9]	[10]	[11]	[12]	[13]	[14]	[15]	[16]	[17]
S5 0014+813	3.336	7.5e9	1350	2878	7.2e4	829	0.85	14	3	0.042	3.5	45	2e3	1	–1	3.3
B0222+185 H	2.690	1.5e9	360	725	1.8e4	52.7	0.27	14	3	0.065	3.3	35	2e3	3.2	1	3.2
B0222+185 L	2.690	1.5e9	360	725	1.8e4	52.7	0.27	14	3	0.032	4.7	17	2e3	3	1.2	3.2

TABLE 2

INPUT PARAMETERS USED TO MODEL THE SED. COL. [1]: SOURCE NAME. H INDICATES THE HIGHER STATE, L THE LOWER; COL. [2]: REDSHIFT; COL. [3]: BLACK HOLE MASS IN SOLAR MASS UNITS; COL. [4]: DISTANCE OF THE BLOB FROM THE BLACK HOLE IN UNITS OF 10^{15} CM. THE SIZE OF THE EMITTING REGION IS DEFINED AS $R_{\rm blob} = \psi R_{\rm diss}$, WHERE $\psi = 0.1$rad IS THE JET APERTURE ANGLE; COL. [5]: RADIUS OF THE BLR IN UNITS OF 10^{15} CM; COL. [6]: RADIUS OF THE TORUS IN UNITS OF 10^{15} CM; COL. [7]: DISK LUMINOSITY IN UNITS OF 10^{45} ERG S^{-1}; COL. [8]: DISK LUMINOSITY IN UNITS OF THE EDDINGTON LUMINOSITY; COL. [9]: BULK LORENTZ FACTOR; COL. [10]: VIEWING ANGLE (DEGREES); COL. [11]: POWER INJECTED IN THE BLOB CALCULATED IN THE COMOVING FRAME, IN UNITS OF 10^{45} ERG S^{-1}; COL. [12]: MAGNETIC FIELD IN GAUSS; COL. [13], [14]: BREAK AND MAXIMUM RANDOM LORENTZ FACTORS OF THE INJECTED ELECTRONS; COL. [15]: RANDOM LORENTZ FACTORS OF THE ELECTRONS COOLING IN R/c; COL. [16] AND [17]: SLOPES OF THE INJECTED ELECTRON DISTRIBUTION [$Q(\gamma)$] BELOW AND ABOVE $\gamma_{\rm b}$. THE SPECTRAL SHAPE OF THE CORONA IS ASSUMED TO BE $\propto \nu^{-1}\exp(-h\nu/150\,{\rm keV})$.

Source	$\log P_{\rm r}$	$\log P_{\rm B}$	$\log P_{\rm e}$	$\log P_{\rm p}$
[1]	[2]	[3]	[4]	[5]
S5 0014+813	46.4	47.2	44.6	47.3
B0222+185 H	46.5	46.0	45.5	48.2
B0222+185 L	46.1	46.3	45.3	48.1

TABLE 3

LOGARITHM OF THE JET POWER IN DIFFERENT FORMS. COL. [1]: SOURCE NAME. H INDICATES THE HIGHER STATE, L THE LOWER; COL. [2]: JET POWER IN THE FORM OF RADIATION; COL. [3]: JET POWER CONNECTED TO POYNTING FLUX; COL. [4]: JET POWER IN FORM OF BULK MOTION OF ELECTRONS; COL. [5]: JET POWER IN FORM OF BULK MOTION OF PROTONS (ASSUMING ONE COLD PROTON PER EMITTING ELECTRON).

Ghisellini et al. 2014). Therefore, assuming one proton per relativistic electron is reasonable to explain the observed jet features and its physics.

The emitting regions of both sources are located within the broad line region (and the infrared torus). In this way, the energy density of photons from the broad line region feed the inverse Compton process, together with photons from the torus. The inverse Compton process is dominated by external Compton instead of synchrotron–self Compton, as expected in FSRQs. Tagliaferri et al. (2015) obtained the same result for two other $z > 2$ blazars observed by *NuSTAR*: the emitting regions of both S5 0836+710 and PKS 2149–306 are located between the BLR and IR torus. Their results were obtained through SED fitting, and were also confirmed on the basis of the variability timescales obtained with two *NuSTAR* observations per source.

5. DISCUSSION

Blazars are characterised by their prominent relativistically boosted jet emission. They usually show prominent high–energy emission, which results in high γ–ray luminosities, well detected by instruments like *Fermi*/LAT. In some cases, though, blazars are not detected in such energy bands. This is the case for S5 0014+318 and B0222+185. Even if lacking a high–energy detection, the Compton bump can be observed in the X–ray frequency range, but a detection in the soft X–rays usually is not enough to determine the relativistic jet features of a blazar, nor its orientation. S5 0014+318 and B0222+185 were detected by *Swift*/BAT, but these data were not precise enough to derive exact estimates of the bulk Lorentz factors and viewing angles. Figures 1 and 2 show that the *Swift*/BAT data do not have enough precision to constrain the hard X–ray slope. *NuSTAR*, however, provides a broad–band, precise measurement for both sources, confirming that both blazars are seen at small viewing angles, i.e. their jets are directed along our line of sight. Both sources also host massive central black holes (both with $M_{\rm BH} > 10^9 M_{\odot}$).

5.1. *Variability*

Looking in detail at the broad–band SEDs of these two objects, we see some interesting differences. Both sources show the two humps, i.e. the signature of aligned jet emission, while in the IR–optical–UV band, the accretion disk emission dominates over the non–thermal jet emission. Comparing the two panels of Figure 2, it can be noticed that S5 0014+318 and B0222+185 also show different variability behaviours. They were both observed in two epochs separated by ~ 1 month. S5 0014+318 does not show flux or spectral variation between the two observations, and the new data are consistent with archival data. Only the *Swift*/BAT detection could suggest a different state of the source, but due to the large uncertainty we cannot draw any strong conclusion.

B0222+185, instead, shows a clear variation of the X–ray flux between the two *Swift*/XRT + *NuSTAR* observations: in December 2014 the source was in a higher state, compared to both January 2015 and archival data. The right panel of Figure 1 shows the peak of the high–energy hump shifted towards *higher* frequencies in the *higher* state. This is opposite to the general trend displayed by the blazar sequence.

Such behaviour is not uncommon in rapidly varying FSRQs: although they follow the blazar sequence when considering different sources, an individual object can behave opposite to the sequence itself while varying. According to the model shown in Figure 2, the B0222+185 variability can be described by a variation in the injected power (see second and third lines of Table 2), accompanied by $\gamma_{\rm b}$ increasing in the high state.

Another remarkable example of this kind of variation, very similar to the one showed by B0222+185, but much more pronounced, has recently been seen for S5 0836+710 (Ciprini et al. 2015; Vercellone et al. 2015; Giroletti et al. 2015) during its August 2015 γ–ray flare, which triggered observations at X–ray and radio frequencies. The amplitude of the flux variation was huge in the *Fermi*/LAT band (factor 65 greater than the average flux reported in the third *Fermi*/LAT catalog of Acero et al. 2015) and rather modest in the high energy part of the *Swift*/XRT band. This implies that the X–ray flux had to change more at larger energies, to connect to the enhanced γ–ray flux, and that the peak frequency of the high energy hump must be "bluer" than what was displayed during the *NuSTAR* observation described in Tagliaferri et al. (2015). In other words: if *NuSTAR* had followed the August 2015 flare of S5 0836+710, it likely would have detected a clear flux and spectral variation, leading to a predicted shift of the high energy hump towards higher frequencies even in the absence of γ–ray data. The right panel of Figure 1 shows that *Swift*/XRT would not have been able to discriminate between the two states of B0222+185, while *NuSTAR* distinguishes them clearly. We conclude that:

- observations in the hard X–ray band are not only instrumental to discover the most powerful blazars (that requires a survey of a large portion of the sky), but also to detect large flux variations that occur around the MeV energy band and are not noticeable in the classic 0.3–10 keV band, nor at energies beyond 100 MeV, where the source could go undetected even during a large flare; and

- repeated hard X–rays observations on timescales of a few weeks up to 1–2 months are efficient to spot variability in high–redshift blazars. We managed to see variability in B0222+185, with similar features as the already observed variable FSRQs S5 0836+710 and PKS 2149–306 discussed by Tagliaferri et al. (2015).

5.2. *Jets and accretion of the two most powerful blazars*

We now aim to frame S5 0014+318 and B0222+185 within the larger blazar picture. We consider them in the jet–accretion correlation scenario. Ghisellini et al. (2014) found that in blazars the jet power not only correlates with the accretion power, but it is even larger. This suggests that accretion is strongly related to jet power, implying a role in jet production. At the same time, the fact that jet power is larger than accretion power tells us that some other process must play a role in the jet launch and acceleration. Black hole spin is the best candidate to play such a role. This result was obtained by studying a sample of *Fermi*–detected blazars, for which Shaw et al. (2012; 2013) obtained optical spectra. Ghisellini et al. (2014) selected all the objects with broad emission lines, in order to have a proxy of accretion luminosity, and compared jet and accretion power for the 226 blazars in this sample. However, this sample did not include the most extreme blazars known, leaving open the questions: *how does the jet–accretion relation look in the case of the most powerful blazars?* Does the power balance change when accretion or jet emission are extreme? These questions will guide us in the following discussion.

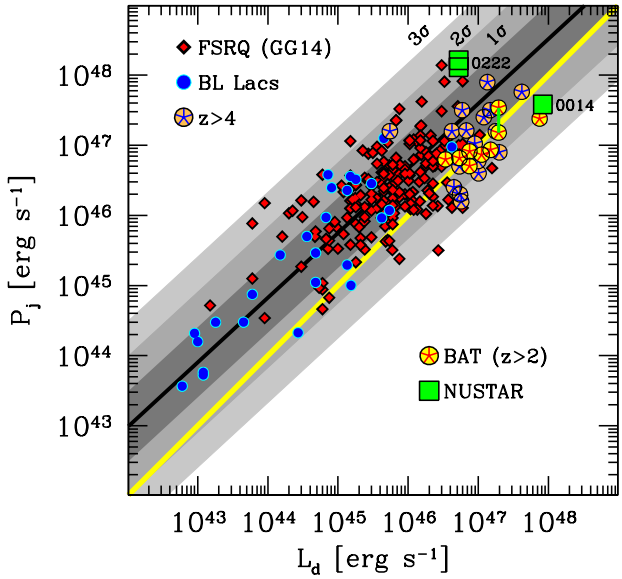

FIG. 3.— Total jet power as a function of accretion disk luminosity in blazars. Red (outlined in black) diamonds and blue filled circles are respectively FSRQs and BL Lacs from Ghisellini et al. (2014). Circled asterisks are high–redshift, non γ–ray detected blazars: pink–filled circles with blue asterisks are all the known $z > 4$ blazars (see Ghisellini et al. 2015), yellow–filled circles with red asterisks are the $z > 2$ blazars detected by *Swift*/BAT. Green filled squares are S5 0014+318 and B0222+185 (both states) as labelled, observed by *NuSTAR* for this work. Note that the latter are the two blazars with the most luminous accretion disk (S5 0014+318) and the most powerful jet (B0222+185). The black line and grey stripes are the best fit relation of γ–ray detected blazars from Ghisellini et al. (2014), along with the 1σ, 2σ and 3σ dispersions. The yellow line is the one–to–one correlation. S5 0836+710 underwent a prominent γ–ray flare, and therefore it has been plotted with the jet powers of both its average and flaring states. The two states are connected with a green line. This suggests that part of the spread could be due to different states of the single sources, along with flaring episodes. The jet power is calculated as the sum of the different components listed in Table 3. Note that the very powerful blazars we added to the original sample by Ghisellini et al. (2014) are located within 2σ from the γ–ray detected jet–accretion relation. This means that also in the most powerful sources the jet power correlates with accretion luminosity, but it is larger than the accretion power, leading to an important role of black hole spin in jet launching.

First we add to the original blazar sample the sources expected to be the most powerful. To this aim we select the $z > 2$ blazars detected by *Swift*/BAT and all known high–redshift ($z > 4$) blazars. The BAT sensitivity limit is not very deep, and at high redshift it can detect mainly the most powerful sources, whose high–energy components peak in the ∼MeV range. BAT detected 10 $z > 2$ blazars, including S5 0014+318 and B0222+185, that we add to the blazar sample of Ghisellini et al. (2014). We also include all the known blazars at $z > 4$, as listed in Ghisellini et al. (2015). Being the highest redshift blazars currently known, they are expected to be among the most powerful blazars. They are not present in the BAT blazar catalog because their distance makes their hard X–ray flux too weak for a detection with BAT. Since most of them were selected starting from optical catalogs, they are likely very powerful in accretion luminosity.

Figure 3 shows how these samples are located in the overall jet–accretion relation, along with S5 0014+318 and B0222+185. The total jet power (calculated as the sum of different jet power components listed in Table 3) is plotted as a function of the disk luminosity. The grey stripes show the best fit of the sample by Ghisellini et al. (2014). Note that the powerful blazars we add in this work are all located within the 2σ dispersion of the previous correlation. This means that they still follow the jet–accretion relation found by Ghisellini et al. (2014), even if they are among the most powerful sources in the set.

S5 0014+318 and B0222+185 can be considered the two most extreme sources: respectively, they are the blazars with the most luminous disk and the most powerful jet. Still, they are close enough to the known jet–accretion correlation, to be less than 2σ from the Ghisellini et al. (2014) result. Thus we conclude that even the most powerful blazars follow the same jet–accretion relation as the γ–ray detected bulk sample. The second interesting conclusion that we can draw from this comparison is that *NuSTAR* is once again confirmed to be the most suitable telescope to study the most powerful blazars in our Universe.

6. CONCLUSIONS

The simultaneous X–ray observations of S5 0014+318 and B0222+185 performed with *Swift*/XRT and *NuSTAR* gave us an interesting insight into the jet emissions of these two sources. We confirmed their blazar nature, with a refined estimate of their bulk Lorentz factors and viewing angles, supported by more precise sets of parameters (Tables 2 and 3). The accretion disk fitting to a more complete data set gave us the possibility to refine our previous estimates of the black hole mass and accretion luminosity of these two sources, implying fast accreting objects with extreme masses of $> 10^9 M_\odot$.

The overall SED modelling allowed us to estimate the jet power and accretion disk luminosity, allowing a comparison of these two sources with the overall blazar jet–accretion relation. The two sources are among the most powerful blazars known, and they populate the highest disk luminosity and jet power part of the jet–accretion correlation (Ghisellini et al. 2014; Figure 3). It is remarkable that a sample formed by the most powerful blazars known is still within 2σ from the correlation derived from a sample of blazars whose γ–ray flux was averaged over two years. The mechanisms governing the jet formation

and evolution in the most extreme sources must not be different from the processes powering the more moderate objects. S5 0014+318 and B0222+185 themselves are consistent with the relation derived from the γ–ray blazars, even if they are the blazars with the most luminous accretion disk and the most powerful jet, respectively.

We found a different variability behaviour between the two sources: while S5 0014+318 did not vary in the two observation epochs separated by ~ 1 month, B0222+185 shows a clear variation, with an amplitude larger at larger frequencies. This last feature is the main reason why *NuSTAR* is such a crucial instrument to study high–redshift and powerful blazars. A soft X–ray telescope alone could not see a variability event like the one shown by B0222+185: *NuSTAR* instead observes at frequencies where the amplitude of a flaring activity is large enough to be seen. Were we lacking the γ–ray signature of a flare, *NuSTAR* could do the job.

ACKNOWLEDGEMENTS

We acknowledge financial support from the ASI-INAF grant I/037/12/0. This work made use of data from the *NuSTAR* mission, a project led by the California Institute of Technology, managed by the Jet Propulsion Laboratory, and funded by the National Aeronautics and Space Administration. We thank the *NuSTAR* Operations, Software and Calibration teams for support with the execution and analysis of these observations. This research has made also use of the *NuSTAR* Data Analysis Software (NuSTARDAS) jointly developed by the ASI Science Data Center (ASDC, Italy) and the California Institute of Technology (Caltech, USA). This publication makes use of data products from the *Wide–field Infrared Survey Explorer*, which is a joint project of the University of California, Los Angeles, and the Jet Propulsion Laboratory/California Institute of Technology, funded by the National Aeronautics and Space Administration. Part of this work is based on archival data, software or on–line services provided by the ASI Data Center (ASDC). This research has made use of the XRT Data Analysis Software (XRTDAS) developed under the responsibility of the ASI Science Data Center (ASDC), Italy.

REFERENCES

Acero et al. 2015, ApJS, 218, 23
Ajello M., Costamante L., Sambruna R.M. et al., 2009, ApJ, 699, 603
Ajello M., Alexander D.M., Greiner J., Madejski G.M., Gehrels N. & Burlon D., 2012, ApJ, 749, 21
Atwood W.B. Abdo A.A. Ackermann M., et al. 2009, ApJ, 697, 1071
Baumgartner W.H., Tueller J., Markwardt C.B., Skinner G.K., Barthelmy S., Mushotzky R.F., Evans P.A. & Gehrels N., 2013, ApJS, 207, 19
Bechtold J., Elvis M., Fiore, F. et al., 1994, AJ, 108, 374
Burrows D., Hill J., Nousek J., et al., 2005, Space Sci. Rev. 120, 165
Calderone G., Ghisellini G., Colpi M, Dotti M. 2013, MNRAS, 431, 210
Chiaberge M., Capetti A. & Celotti A., 1999, A&A 349, 77
Cash W. 1979, ApJ, 228, 939
Ciprini S. for the *Fermi*/LAT collaboration, 2015, ATel 7870
Fitzpatrick E.L. & Massa D. 2009, ApJ, 699, 1209
Fossati G., Maraschi L., Celotti A., Comastri A. & Ghisellini G. 1998, MNRAS, 299, 433
Ghisellini G., Della Ceca R., Volonteri M. et al. 2010, MRAS, 405, 387
Ghisellini G., Foschini L., Volonteri M., Ghirlanda G., Haardt F., Burlon D. & Tavecchio, F. 2009, MNRAS, 399, L24
Ghisellini G., Haardt F., Ciardi B., Sbarrato T., Gallo E., Tavecchio F. & Celotti A. 2015, MNRAS, 452, 3457
Ghisellini G. & Tavecchio F., 2009, MNRAS, 397, 985
Ghisellini G., Tavecchio F., Foschini L. & Ghirlanda G. 2011, MNRAS, 414, 2674
Ghisellini G., Tavecchio F., Maraschi L., Celotti A. & Sbarrato T. 2014, Nature, 515, 376
Ghisellini G. 2012, MNRAS, 424, L26
Giommi P., Padovani P., Polenta G., et al. 2012, MNRAS, 420, 2899
Giroletti M., Righini S., Bach U., D'Ammando F., Orienti M., Raiteri C.M. & Villata M., 2015, ATel 7890
Harrison F.A., Craig W.W., Christensen F.E., et al. 2013, ApJ, 770, 103
Kalberla P.M.W., Burton W.B., Hartmann D., et al. 2005, A&A, 440, 775
Madsen K.K., Harrison F.A., Markwardt C.B., et al. 2015, ApJS, 220, 8
Nemmen R.S., Georganopoulos M., Guiriec S., Meyer E.T., Gehrels N. & Sambruna R.M. 2012, Science, 338, 1445
Poole T.S., Breeveld A.A., Page M.J., et al. 2008, MNRAS, 383, 627
Roming P.W.A., Kennedy T.E., Mason K.O., et al. 2005, SSRv, 120, 95
Sbarrato T., Ghisellini G., Maraschi L. & Colpi M. 2012, MNRAS, 421, 1764
Sbarrato T., Ghisellini G., Nardini M., et al. 2013, MNRAS, 433, 2182
Schlafly E.F., & Finkbeiner D.P. 2011, ApJ, 737, 103
Schlegel D.–J., Finkbeiner D.P. & Davis M. 1998, ApJ, 500, 525
Shakura N.I. & Sunjaev R.A. 1973, A&A, 24, 337
Shaw M.S., Romani R.W., Cotter G., et al. 2012, ApJ, 748, 49
Shaw M.S., Romani R.W., Cotter G., et al. 2013, ApJ, 764, 135
Sikora M. & Madejski G.M. 2000, ApJ, 534, 109
Tagliaferri G., Ghisellini G., Perri M. et al., 2015, ApJ, 807, 167
Vercellone S., Romano P., Raiteri C.M. & Villata M., 2015, ATel 7898
Wright E.L., Eisenhardt P.R.M., Mainzer A.K., et al. 2010, AJ, 140, 1868

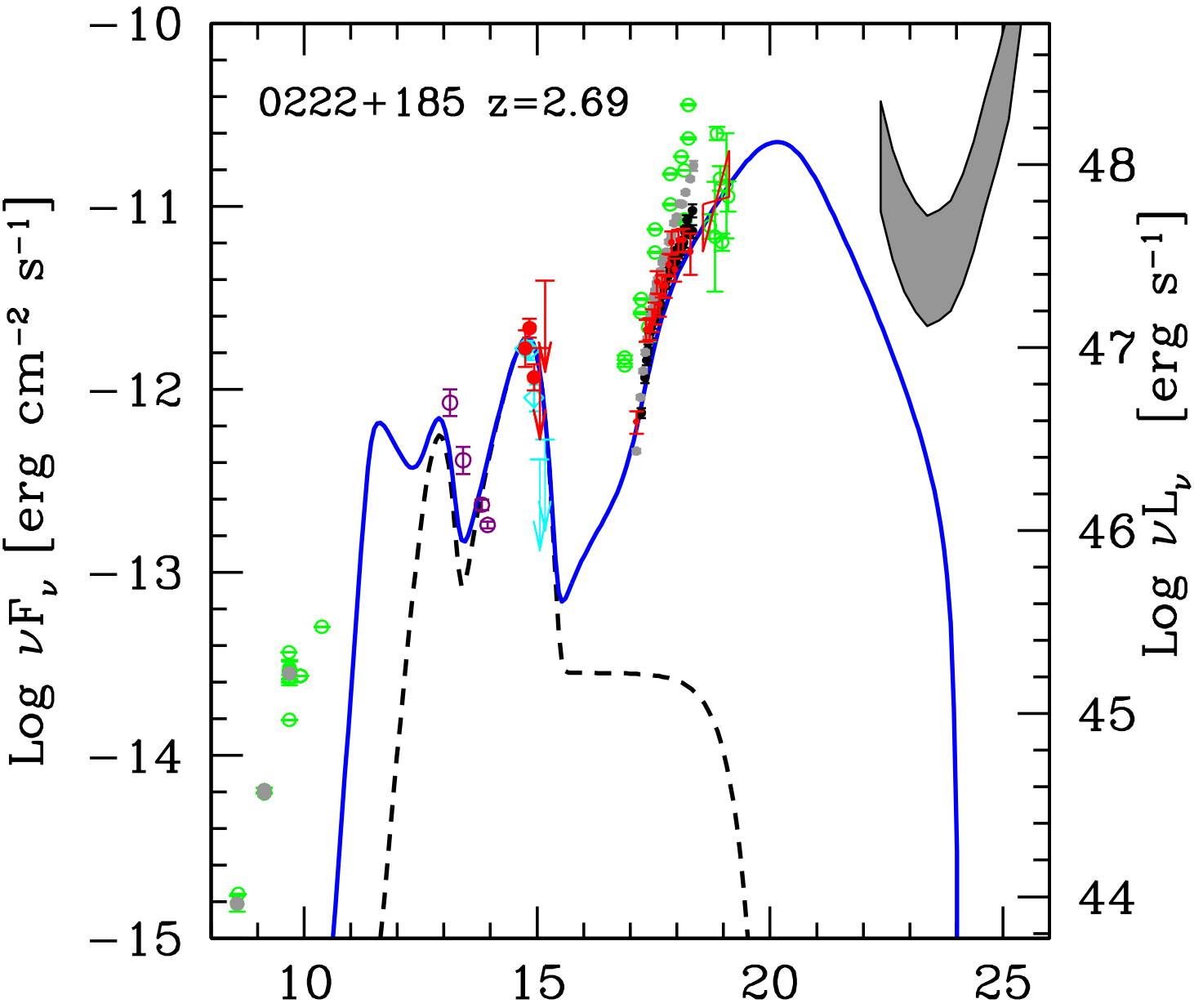
0222+185 z=2.69
Log νF_ν [erg cm^-2 s^-1]
Log νL_ν [erg s^-1]
−10
−11
−12
−13
−14
−15
48
47
46
45
44
10
15
20
25